



Article

The migration and occupation of Li⁺ and Na⁺ in illite and montmorillonite during the heating process

Nanominerals and mineral nanoparticles – thematic issue

Zhenxiao Wu¹, Shangying Li^{1,2}, Yang Wang¹ and Hongfei Cheng¹ 

¹School of Earth Science and Resources, Chang'an University, No. 126 Yanta Road, Xi'an 710054, China; and ²School of Land Engineering, Chang'an University, No. 126 Yanta Road, Xi'an 710054, China

Abstract

The impact of temperature on the migration of cations within layers of clay minerals is of profound significance for the design and practical application of materials derived from clay minerals. This study focuses on Li⁺ and Na⁺ as representative cations, together with illite (Ilt) and montmorillonite (Mnt) as representative clay minerals. The study investigates the behaviour of cation migration and occupation within clay minerals across varying temperatures. A series of samples were prepared meticulously by immersing illite and montmorillonite in Li⁺ and Na⁺ solutions, subsequently subjecting them to different temperatures (unheated, 100, 150, 200, 250 and 300°C) for 24 h. Through the use of techniques such as X-ray diffraction (XRD), cation exchange capacity (CEC), Fourier-transform infrared spectroscopy (FTIR), magic angle rotating solid nuclear magnetic resonance spectroscopy (MAS NMR), and X-ray photoelectron spectroscopy (XPS), the study discerns structural transformations in illite and montmorillonite, and tracks the migration and occupation of Li⁺ and Na⁺. The findings reveal that following heating, Na⁺ and Li⁺ do not infiltrate the lattice of illite. For montmorillonite, Na⁺ also does not migrate into the montmorillonite lattice, however, in contrast, Li⁺ does exhibit migration into this lattice. Notably, the migration and occupation of interlayer Li⁺ within montmorillonite exhibit discernible temperature dependence. Specifically, upon reaching 150°C, interlayer Li⁺ migrate to ditrigonal cavities within the tetrahedral layers. As the temperature elevates to 200°C, Li⁺ further permeate vacant octahedral sites through the ditrigonal cavities, culminating in the formation of a localised trioctahedral structure.

Keywords: montmorillonite; illite; Li⁺; Na⁺; cation migration; cation occupation

(Received 18 December 2023; accepted 29 March 2024; Accepted Manuscript published online: 25 April 2024)

Introduction

Clay minerals have diverse applications across different disciplines, including agriculture, medicine, and the environment, with a notable role as repositories for radioactive waste storage (Komadel *et al.*, 2005; Madejová *et al.*, 2006; Zhao *et al.*, 2022a). Most clay minerals assume a layered silicate structure, and these layers can be categorised as 1:1 and 2:1 type (Cheng *et al.*, 2010; Li *et al.*, 2022). The 1:1 type includes one tetrahedral sheet and one octahedral sheet (Cao *et al.*, 2021), whereas the 2:1 type includes two tetrahedral sheets with one octahedral sheet situated between them (Bodart *et al.*, 2018). The octahedra come in two forms: (1) dioctahedral, wherein two thirds of the octahedral cation centres are occupied by cations; and (2) trioctahedral, where all octahedral cation positions are filled (Gao, 2017; Wu *et al.*, 2022). Both illite and montmorillonite are 2:1 layer clay minerals displaying dioctahedral structures (Gournis *et al.*, 2008; Zhao *et al.*, 2022b).

Negative charges within the structural layer of illite and montmorillonite originate from isomorphous substitution of Al³⁺ in the octahedral sheet by Fe²⁺, Mg²⁺, etc., alongside limited Al³⁺ replacement for Si⁴⁺ in tetrahedral sheets. The resulting negative charge is offset by exchangeable cations (e.g. Na⁺ and K⁺) at sheet edges and within interlayers (Chen and Wang, 2007; Wang *et al.*, 2011; Jeldres *et al.*, 2019; Zhao *et al.*, 2022b).

An accurate understanding of the interaction mechanism between mineral lattices and interlayer cations subsequent to heat or hydrothermal treatment is crucial for designing and employing clay-mineral-based materials, particularly in radioactive waste storage where elevated temperatures can prompt some interlayer cations to infiltrate clay structures, inducing mineral structural layer collapse and a significant reduction in containment efficacy for the radioactive waste (Theng *et al.*, 1997; Alba *et al.*, 1998). Studies have revealed that heating clay minerals within the range of 200–300°C can result in interlayer cation immobilisation, leading to irreparable mineral structural layer collapse, known as the Hofmann–Klemen effect (Schultz, 1969; Greene-Kelly, 1995). Three viewpoints exist regarding interlayer cation occupation sites within the Hofmann–Klemen effect: (1) cations infiltrate ditrigonal cavities in tetrahedral layers (Tettenhorst, 1962; Beaufort *et al.*, 2001; Bodart *et al.*, 2018); (2) cations inhabit vacant octahedral

Corresponding author: Hongfei Cheng; Email: h.cheng@chd.edu.cn

Guest Editor: Qingze Chen

This paper is part of a thematic set on Nanominerals and mineral nanoparticles

Cite this article: Wu Z., Li S., Wang Y. and Cheng H. (2024) The migration and occupation of Li⁺ and Na⁺ in illite and montmorillonite during the heating process. *Mineralogical Magazine* 88, 536–545. <https://doi.org/10.1180/mgm.2024.27>

positions (Farmer and Russell, 1967; Gates *et al.*, 2000; Stackhouse and Coveney, 2002); and (3) cations migrate to both sites (Russell and Farmer, 1964; Komadel *et al.*, 2005) (Fig. 1). Notably, research on montmorillonite heating commonly involves investigations into interlayer cation migration locations (Karakassides *et al.*, 1999; Madejová *et al.*, 1999a). Using infrared spectroscopy, Tettenhorst (1962) observed interlayer Li^+ migration into ditrigonal cavities within tetrahedral layers upon heating montmorillonite to 300°C, with no migration into vacant octahedra. Luca and Cardile (1988) used a ^{57}Fe atomic probe to ascertain that Li^+ primarily occupied tetrahedral sites during montmorillonite heating. Infrared spectroscopy-based findings by Farmer and Russell (1967) indicated Li^+ migration into vacant octahedral positions during heating, with the remaining interlayer Li^+ interacting with structural OH groups to release H^+ . Density functional theory (DFT) calculations by Ebina *et al.* (1999) postulated interlayer Li^+ migration from interlayers into ditrigonal cavities and vacant octahedral positions in montmorillonite, occurring at temperatures of 250–350°C, with respective migration rates of 60% and 40%. Furthermore, studies have reported cation migration during montmorillonite heating for other cations (e.g. Cd^{2+} , Mg^{2+} , Cu^{2+} and Ni^{2+}). Based on infrared spectroscopy, Madejová *et al.* (1999b) investigated Cu^{2+} and Cd^{2+} migration between montmorillonite layers after heating, revealing Cd^{2+} is incapable of migrating to tetrahedral and octahedral structures, and Cu^{2+} has limited migration into ditrigonal cavities within tetrahedral layers, without further penetration into vacant octahedral positions. It is evident that cationic properties, including ionic radius and valence, significantly impact cation migration sites in clay minerals. Moreover, mineral species can also influence cation transport patterns between layers. However, few studies have examined interlayer cation occupation in distinct clay mineral types following heating. Thus, this study has selected Li^+ and Na^+ as representative cations and illite and montmorillonite as representative clay minerals. The thermal migration and occupation characteristics of interlayer cations in clay minerals were investigated using X-ray diffraction (XRD), Fourier transform infrared spectroscopy (FTIR), magic angle rotating solid nuclear magnetic resonance spectroscopy (MAS NMR) and X-ray photoelectron spectroscopy (XPS).

Experimental

Materials

For this investigation, the clay minerals illite and montmorillonite were selected (symbols Ilt and Mnt, respectively, using Warr, 2020). Illite was obtained from the Carboniferous Benxi Formation,

located in Kou Town, Xianyang City, Shaanxi Province, whereas montmorillonite was procured from Xianding Biotechnology Co. Ltd. To eliminate soluble impurities, the clay mineral samples underwent a thorough process of triple rinsing using deionised water. Subsequently, they were dried in an oven at 50°C for 24 h and further ground in an agate mortar until reaching a powder consistency with a 200 mesh particle size. The Na^+ and Li^+ solutions were prepared by dissolving Na_2SO_4 and Li_2SO_4 , respectively, in ultrapure water. The analytical grade Na_2SO_4 and Li_2SO_4 were purchased from Tianli chemical reagent Co., Ltd. (Tianjin, China) and Komio Chemical Reagents Co., Ltd. (Tianjin, China), respectively. To prepare Na^+ -saturated montmorillonite and Li^+ -saturated montmorillonite (Na^+ -Mnt and Li^+ -Mnt), 4.00 g of montmorillonite was added to 100 mL of Na^+ (1M) and Li^+ (1M) solutions, respectively. These solutions were agitated for a duration of 2 h at 25°C and 50 r/min. Subsequently, the samples underwent centrifugation at 10,000 rpm for 10 min to facilitate solid–liquid separation. The isolated solids were air-dried under natural conditions at ~25°C. The dried montmorillonite samples were then exposed to various temperatures for 24 h. The resulting specimens were designated as M-Mnt25, M-Mnt100, M-Mnt150, M-Mnt200, M-Mnt250 and M-Mnt300. In this nomenclature, M signifies either Na^+ or Li^+ , M-Mnt25 denotes a sample that was at room temperature (not subjected to heating), and M-Mnt100 signifies a sample heated to 100°C. Additionally, control samples were produced by mixing 4.00 grams of illite with 100 mL solutions of Na^+ (1M) and Li^+ (1M), respectively. The resulting control samples were named M-Ilt25, M-Ilt100, M-Ilt150, M-Ilt200, M-Ilt250 and M-Ilt300.

Characterisations

The major chemical compositions of illite and montmorillonite were analysed using an X-ray fluorescence spectrometer (XRF, Shimadzu LAB CENTER XRF-1800). Cation exchange capacities (CEC) in samples were determined by extraction with ammonium acetate solution (1M) at pH 7. A 100 mg sample was rinsed triple with deionised water to remove water-soluble cations and collect solid. The solid was dispersed in 20 mL ethanol, then 20 mL ammonium acetate solution was added, and the extraction solution was collected after standing for 24 h. Subsequently, 20 mL deionised water was added to the remaining solid and the extraction solution was collected after 24 h. The extraction process was repeated three times, and all extraction solutions of the same sample were mixed. The cation concentration (Na^+ and Li^+) in the solution was determined by inductively coupled plasma optical emission spectrometry (ICP-OES, Agilent 5110).

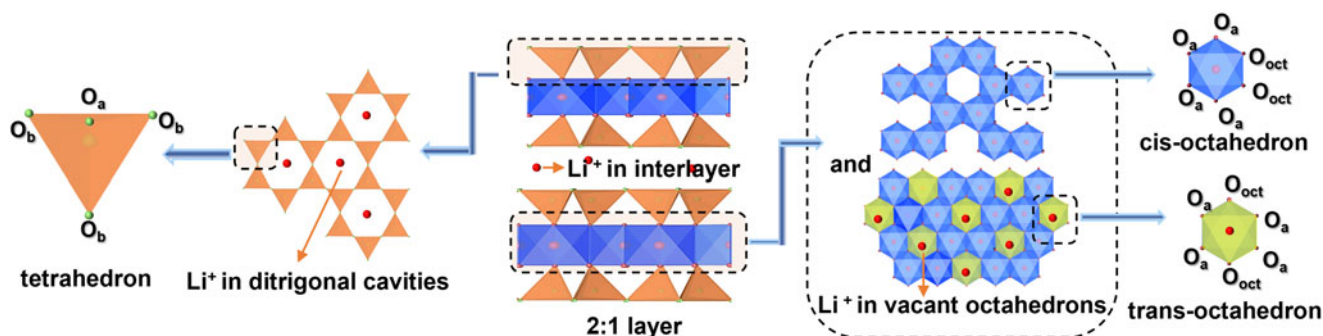


Figure 1. Schematic diagram of possible occupation sites of Li^+ in clay minerals with a 2:1 layer type of two tetrahedral sheets (SiO_4 tetrahedra) with one octahedral sheet in between. Three possible Li^+ occupation sites are: in ditrigonal cavities; in the interlayer; and in vacant octahedral positions (Bodart *et al.*, 2018; Zhao *et al.*, 2023).

X-ray diffraction patterns were obtained using a Shimadzu XRD-6100 powder diffractometer. The instrument employed a Cu target as the source (40 kV voltage and 30 mA current) and scanned within the 2θ range of $2\text{--}70^\circ$ at a scanning speed of $4^\circ/\text{min}$. FTIR spectra were acquired using the KBr pressing method. A Thermo Fisher Nicolet iS5 FTIR spectrometer was employed for data collection, utilising 1 mg of sample powder and 100 mg of spectrographic pure KBr powder. This mixture was ground thoroughly for 15 min and subsequently pressed into transparent flakes. Infrared spectral data were gathered across the range of $4000\text{--}400\text{ cm}^{-1}$, involving 32 scans at a resolution of 4 cm^{-1} . MAS NMR spectral data for ^{27}Al , ^{29}Si and ^7Li were obtained using a JEOL ECZ600R/S3 NMR spectrometer from JEOL RESONANCE, Japan. Resonance frequencies were 156.39 MHz for ^{27}Al , 119.20 MHz for ^{29}Si , and 233.08 MHz for ^7Li . Single-pulse decoupled MAS NMR experiments were conducted with a 3.2 mm dual resonance probe, employing magic angle rotation speeds of 15 kHz for ^{27}Al , 12 kHz for ^{29}Si , and 8 kHz for ^7Li . The pulse widths for ^{27}Al , ^{29}Si and ^7Li were set at $\pi/6$, $\pi/2$ and $\pi/4$, respectively, with corresponding pulse delays. Chemical shifts for ^{27}Al , ^{29}Si and ^7Li were referenced externally to solutions of aluminium nitrate ($\text{Al}(\text{NO}_3)_3$), tetramethylsilane (TMS) and lithium chloride (LiCl), respectively. XPS was conducted using a Thermo Fisher Scientific ESCALAB Xi+ X-ray photoelectron spectrometer, equipped with a monochromatised AlK α X-ray source. The full-spectral pass energy is 100 eV with a step size of 1 eV, and the narrow-spectral pass energy is 30 eV with a step size of 0.1 eV. The typical elements Al, Si and Li were examined in this study.

Results and discussion

X-ray diffraction data

The XRD patterns demonstrate the high purity of illite and montmorillonite samples (Fig. 2, Supplementary Fig. S1). Generally, the d values of the $00l$ reflections in minerals are influenced by the radius and hydration status of interlayer cations, whereas the hkl reflections are influenced by mineral layer structures (Alvero *et al.*, 1994; Alba *et al.*, 1998). The positions and intensities of hkl reflections for illite and montmorillonite, heated to different temperatures, remain consistent with their unheated counterparts (Fig. 2). This indicates the absence of changes in the crystal structure of these minerals. The $00l$ reflections for illite show little change when heated to various temperatures. In contrast, the $00l$ reflections for montmorillonite display significant shifts after exposure to different temperatures.

For illite, the $d_{(001)}$ value remains $\approx 10.0\text{ \AA}$ before and after heating, implying that the hydration status and migration behaviour of interlayer cations in illite are not affected by temperature (Fig. 2a,b) (Jeldres *et al.*, 2019). In the case of montmorillonite, the layer spacing of Na^+ -saturated montmorillonite ($\sim 15.3\text{ \AA}$) is slightly larger than that of Li^+ -saturated montmorillonite ($\sim 14.9\text{ \AA}$) in the unheated state. This difference can be attributed to the lower hydration level of Li^+ compared to Na^+ , resulting in slightly larger layer spacing when Na^+ occupies the interlayer. The d values of $00l$ reflections for montmorillonite experience noticeable alterations after exposure to varying temperatures, with a decrease observed in d values as temperature increases (Fig. 2c,d). This may be due to interlayer cations losing ligand water and/or migrating into the montmorillonite lattice. Specifically, for Na^+ -saturated montmorillonite, the $d_{(001)}$ values decrease to ~ 12.5 , ~ 12.4 , ~ 12.4 , ~ 12.4 and $\sim 12.4\text{ \AA}$, whereas for Li^+ -saturated montmorillonite, the

values decrease to approximately ~ 12.4 , ~ 10.9 , ~ 9.9 , ~ 9.6 and $\sim 9.6\text{ \AA}$ after heating to 100, 150, 200, 250 and 300°C , respectively. At 200°C , the layer spacing of Li^+ -saturated montmorillonite falls below 10.0 \AA , aligning with the $d_{(001)}$ value for completely collapsed montmorillonite. Conversely, Na^+ -saturated montmorillonite maintains a layer spacing exceeding 10.0 \AA after exposure to varying temperatures, indicating that heating does not lead to complete crystal structure collapse. Electrostatic interaction exists between silicon–alumininate layers and interlayer cations. Heating can prompt interlayer cations to infiltrate mineral crystal structures, resulting in reduced structural layer negativity, low electrostatic repulsion between layers, and decreased layer spacing. The extent of decrease in the $d_{(001)}$ value suggests that Li^+ exhibits more readiness to infiltrate montmorillonite crystal structures compared to Na^+ .

X-ray fluorescence and cation exchange capacity

The main chemical compositions of illite and montmorillonite are SiO_2 and Al_2O_3 , ranging from 45.8 to 59.5 wt.%, and from 25.7 to 36.1 wt.%, respectively (Table 1). In addition, the K_2O content in illite is higher than that in montmorillonite. By contrast, the contents of $\text{Fe}_2\text{O}_3(\text{tot})$ and MgO in illite are lower than that in montmorillonite.

The CEC of Na^+ and Li^+ in M-Ilt and M-Mnt are shown in Table 2. The amount of exchangeable Na^+ and Li^+ in illite is lower than that in montmorillonite, because the CEC of illite is lower than that of montmorillonite (Zhao and Zhang, 1990). With the increase of temperature, the exchangeable Na^+ and Li^+ in Na^+ -Ilt, Li^+ -Ilt, and Na^+ -Mnt remain almost unchanged. However, exchangeable Li^+ in Li^+ -Mnt gradually decreases, indicating that Li^+ is fixed by montmorillonite upon heating, consistent with the results from XRD.

Fourier-transform infrared spectroscopy

To investigate the migration of cations within illite and montmorillonite, mid-infrared spectroscopy was employed to study the shifts in OH group and Si–O vibrational modes. These vibrational modes include stretching and bending vibrations (Liu *et al.*, 2012; Ai *et al.*, 2013; Qi *et al.*, 2022).

OH stretching and bending vibrations

The FTIR spectra of the unheated samples (Na^+ -Ilt25, Li^+ -Ilt25, Na^+ -Mnt25 and Li^+ -Mnt25) show a prominent absorption band at $\sim 3630\text{ cm}^{-1}$, attributed to the stretching vibration of the OH group coordinated with the cations in octahedral positions (Fig. 3). The stretching vibrational behaviour of the OH group in minerals can be attributed to two factors: (1) the nature of the central atoms in the octahedral coordination with the OH group; and (2) the isomorphic substitution in the lattice structure. In this context, the presence of the tetrahedral top oxygen (O_{ap}) generates local negative charges, which can be counterbalanced by cations entering the lattice. This interplay influences the OH group's stretching vibrations (Madejová *et al.*, 1999a). During the heating process of Na^+ -Ilt, Li^+ -Ilt, and Na^+ -Mnt samples, the OH-stretching vibrational bands remain relatively constant at $\sim 3630\text{ cm}^{-1}$ (Fig. 3a–c). However, the OH stretching vibrational characteristics of Li^+ -Mnt differed noticeably from those of Na^+ -Ilt, Li^+ -Ilt and Na^+ -Mnt. For Li^+ -Mnt heated to 100°C , there is no significant shift in the OH stretching vibration. With further temperature increase, the OH stretching vibrational bands of Li^+ -Mnt150, Li^+ -Mnt200, Li^+ -Mnt250, and

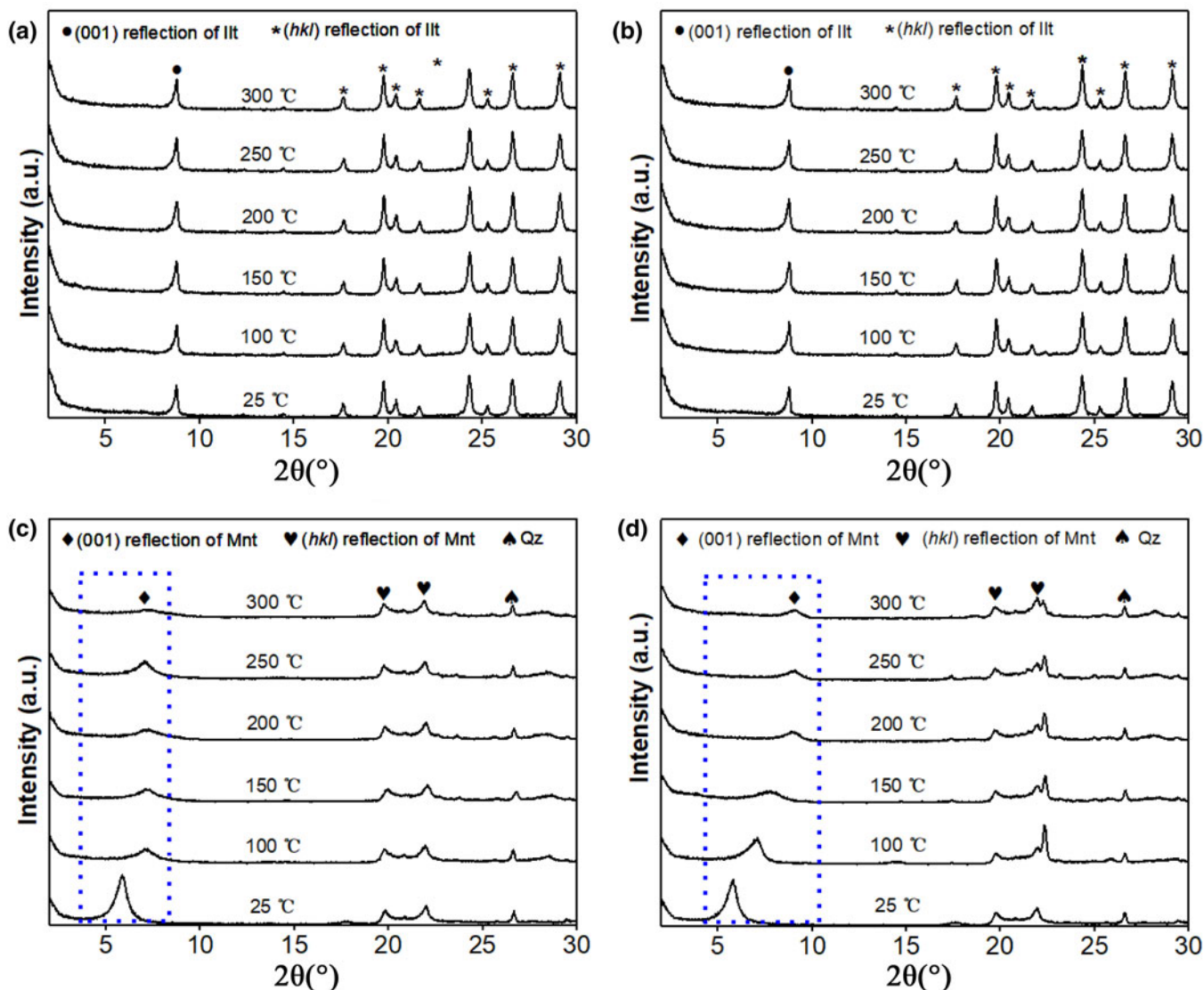


Figure 2. XRD patterns of M-illite and M-montmorillonite subjected to various temperatures: (a) Na⁺-Illite; (b) Li⁺-Illite; (c) Na⁺-Mnt; and (d) Li⁺-Mnt.

Table 1. Major chemical compositions (wt.%) of illite and montmorillonite samples.

Sample	SiO ₂	Al ₂ O ₃	TiO ₂	Fe ₂ O _{3(tot)}	MnO	MgO	CaO	Na ₂ O	K ₂ O	P ₂ O ₅	LOI
Illite	45.8	36.1	1.5	1.0	<0.1	0.5	0.4	<0.1	8.5	<0.1	6.9
Montmorillonite	59.5	25.7	<0.1	4.7	<0.1	3.9	1.5	0.9	0.6	<0.1	1.7

Table 2. CEC values (mmol/g) of Na⁺ and Li⁺ in M-illite and M-montmorillonite subjected to varying temperatures.

Temperature (°C)	Na ⁺ of Na ⁺ -Illite	Li ⁺ of Li ⁺ -Illite	Na ⁺ of Na ⁺ -Mnt	Li ⁺ of Li ⁺ -Mnt
25	0.12	0.13	0.74	0.78
100	0.09	0.12	0.73	0.55
150	0.11	0.13	0.72	0.29
200	0.09	0.11	0.70	0.27
250	0.10	0.12	0.71	0.25
300	0.11	0.12	0.72	0.26

Li⁺-Mnt300 shift to ~3633, ~3634, ~3638 and ~3641 cm⁻¹, respectively. Previous studies have shown that the entry of interlayer cations into the ditrigonal cavities of the tetrahedral layers leads to a shift in OH stretching vibrational bands towards higher wavenumbers (Madejová *et al.*, 2006; Gao, 2017). For the Li⁺-Mnt25 sample, the interactions between OH and O_{ap} form OH...O_{ap} configurations. Upon cation migration into the ditrigonal cavities the interaction between OH and O_{ap} weakens, whereas the interaction between O and H in OH strengthens, leading to a shift in stretching vibrations towards higher wavenumbers (Madejová *et al.*, 1999a). Therefore, it is inferred that interlayer

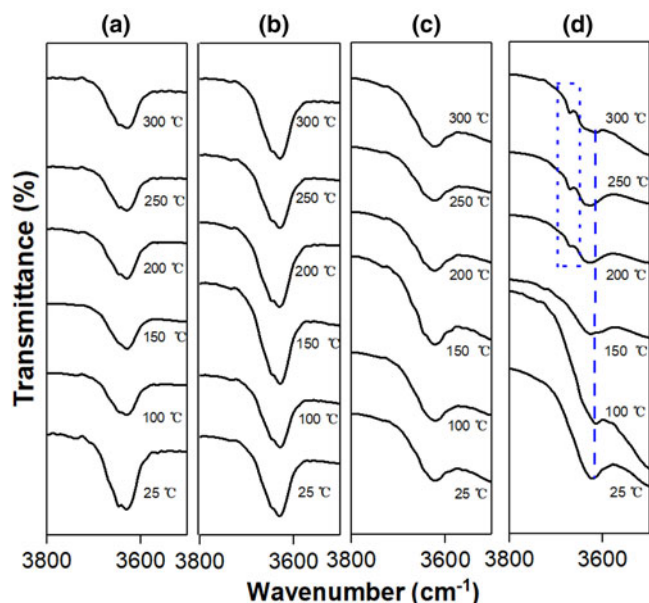


Figure 3. FTIR spectra of OH stretching vibrations for the samples heated to different temperatures: (a) Na⁺-Ilt; (b) Li⁺-Ilt; (c) Na⁺-Mnt; and (d) Li⁺-Mnt.

Li⁺ migrate into the montmorillonite's ditrigonal cavities when heated to 150°C.

Notably, a new vibrational band appears in the FTIR spectrum at $\sim 3671\text{ cm}^{-1}$ upon heating montmorillonite at 200°C (Fig. 3d). Previous studies have indicated that during the heating process, interlayer hydrated Li⁺ could undergo dehydration into the vacant octahedral positions of montmorillonite, forming a local trioctahedral structure (AlMgLi-OH) and giving rise to the emergence of a new OH stretching vibrational band at $\sim 3671\text{ cm}^{-1}$ (Madejová *et al.*, 2006; Jeldres *et al.*, 2019).

The characteristics of hydroxyl-group bending vibrations provide further insights into the behaviour of cation migration during the heating of illite and montmorillonite. The infrared spectra of Na⁺-Ilt25 and Li⁺-Ilt25 show obvious absorption bands at ~ 760 , ~ 832 and $\sim 933\text{ cm}^{-1}$ (Fig. 4a,b). Na⁺-Mnt25 and Li⁺-Mnt25 exhibit pronounced absorption bands at ~ 797 , ~ 844 and $\sim 912\text{ cm}^{-1}$ (Fig. 4c,d), which are presumed to correspond to OH bending vibrations of FeMg-OH, AlMg-OH and AlAl-OH, respectively, in the mineral structure (Gates *et al.*, 2000; Madejová *et al.*, 2000; Skoubris *et al.*, 2013). The positions and intensities of the OH bending vibrational bands remain unchanged during the heating of Na⁺-Ilt, Li⁺-Ilt and Na⁺-Mnt samples (Fig. 4a-c). Conversely, for Li⁺-Mnt, the OH bending vibrational band corresponding to AlAl-OH is not observed after heating at 150°C, and the bending vibrational band intensity of OH in AlMg-OH decrease or even disappear with temperature increasing (Fig. 4d), indicating that Li⁺ can potentially migrate into the montmorillonite lattice.

As mentioned above, the interlayer cations (Na⁺ and Li⁺) do not exhibit migration into the illite lattice. The montmorillonite lattice does not accommodate Na⁺, but can accept inwards migration by Li⁺. This behaviour is predominantly influenced by interlayer cation properties, including ionic radius and valence. Specifically, the ionic radii of Na⁺ and Li⁺ are 0.95 and 0.60 Å, respectively (Madejová *et al.*, 1999a). In comparison to Li⁺, Na⁺ possesses a larger ionic radius, rendering it less prone to entering the montmorillonite lattice. Furthermore, the occupation site of

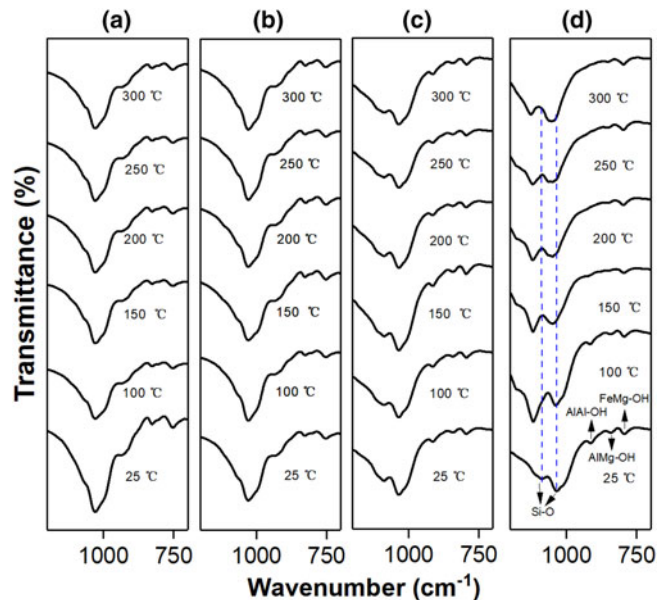


Figure 4. FTIR spectra of OH bending vibrations and Si-O stretching vibrations for the samples heated at different temperatures: (a) Na⁺-Ilt; (b) Li⁺-Ilt; (c) Na⁺-Mnt; and (d) Li⁺-Mnt.

Li⁺ is not limited to a single location and can include both ditrigonal cavities and vacant octahedral sites. Skoubris *et al.* (2013) reported that upon heating, montmorillonite undergoes changes in its hydrated Li⁺ within the interlayers. These ions dehydrate and transition from interlayer positions to occupy ditrigonal cavities, followed by vacant octahedrons.

Si-O stretching and bending vibrations

The migration of interlayer cations from minerals into ditrigonal cavities of tetrahedral layers leads to changes in Si-O stretching and bending vibrational bands. (Clementz and Mortland, 1974; Alvero *et al.*, 1994). This migration also neutralises layer charges, rendering montmorillonite similar to pyrophyllite, a typical uncharged dioctahedral mineral (Karakassides *et al.*, 1999).

Both Na⁺-Ilt25 and Li⁺-Ilt25 exhibit Si-O stretching vibrational bands $\approx 1028\text{ cm}^{-1}$ (Fig. 4a,b). Meanwhile, Na⁺-Mnt25 and Li⁺-Mnt25 display Si-O stretching vibrational bands in the range of 1035–1150 cm^{-1} , with bands at ~ 1039 and $\sim 1093\text{ cm}^{-1}$, respectively (Fig. 4c,d). Notably, heated Na⁺-Ilt and Li⁺-Ilt samples maintain their Si-O stretching vibrational bands, signifying the absence of interlayer cations migrating into the ilmenite lattice structure (Fig. 4a,b). Similarly, the Si-O stretching vibrational bands of Na⁺-Mnt remain unchanged during heating, suggesting no migration of interlayer Na⁺ into the ditrigonal cavities of montmorillonite's tetrahedral layers (Fig. 4c). In contrast, Si-O stretching vibrational bands in the Li⁺-Mnt series shift to higher values after heating (Fig. 4d). Specifically, the $\sim 1039\text{ cm}^{-1}$ band remains relatively stable at 100°C; it shifts to a higher value ($\sim 1043\text{ cm}^{-1}$) at 150°C; then gradually shifts to $\sim 1052\text{ cm}^{-1}$ at 300°C. This alteration indicates the resemblance of montmorillonite's structure to that of pyrophyllite, facilitated by Li⁺ migration during heating. The Si-O stretching band of pyrophyllite is at $\sim 1050\text{ cm}^{-1}$ (Madejová *et al.*, 2006; Xia *et al.*, 2009). Moreover, the band at $\sim 1093\text{ cm}^{-1}$ shifts to $\sim 1115\text{ cm}^{-1}$ at 100°C, further shifting to $\sim 1127\text{ cm}^{-1}$ at 200°C, and eventually progressing to $\sim 1130\text{ cm}^{-1}$ with increasing temperature.

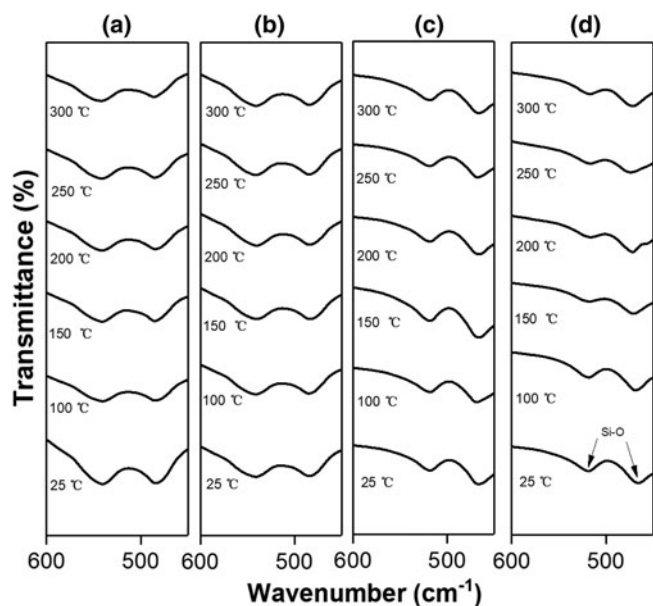


Figure 5. FTIR spectra of Si-O bending vibrations for the samples heated at different temperatures: (a) Na⁺-Ilt; (b) Li⁺-Ilt; (c) Na⁺-Mnt; and (d) Li⁺-Mnt.

In ilmenite, bending vibrational bands of Si-O are mainly located at ~ 537 (Si-O-Al) and ~ 484 cm^{-1} (Si-O-Si). These band positions and intensities remain largely unchanged as temperature increases (Fig. 5a,b). The Si-O-Si and Si-O-Al bending vibrational bands in montmorillonite appear at ~ 467 and ~ 520 cm^{-1} , respectively (Fig. 5c,d). The absorption bands of Na⁺-Mnt remain constant during heating, whereas the Si-O-Al absorption bands of Li⁺-Mnt slightly decrease in intensity with rising temperature.

In summary, interlayer cations in ilmenite do not migrate into its crystal structure. However Na⁺ remains within montmorillonite's interlayers and Li⁺ can penetrate ditrigonal cavities of tetrahedral layers.

Nuclear magnetic resonance and X-ray photoelectron spectroscopy

The XRD and FTIR results indicate that the interlayer Li⁺ in montmorillonite may lose their ligand water when the heating temperature reaches 100°C, and the interlayer Li⁺ migrates into the ditrigonal cavities within the tetrahedral layers when the heating temperature reaches 150°C. To further demonstrate whether Li⁺ can migrate into the vacant octahedral sites of montmorillonite

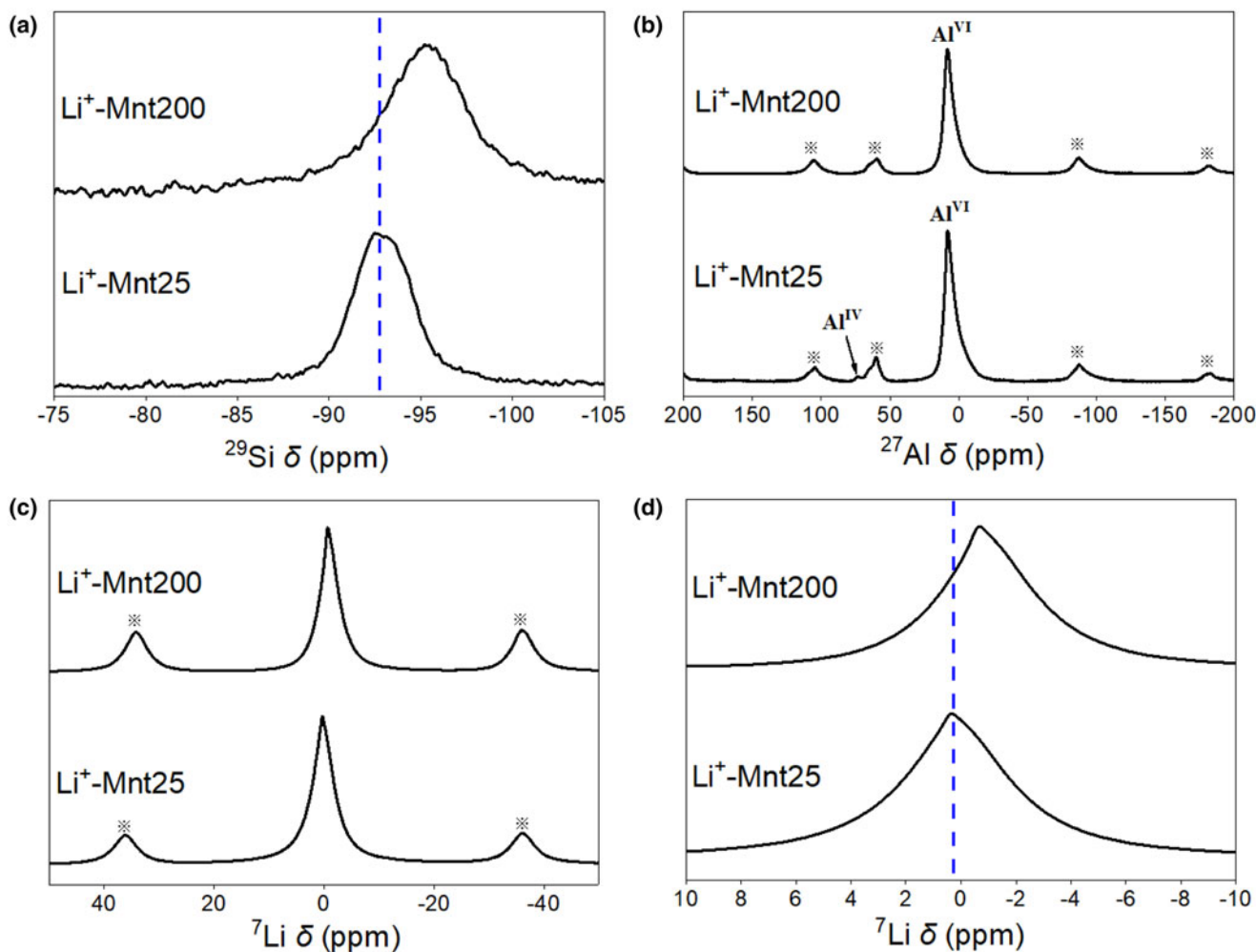


Figure 6. MAS NMR spectra of Li⁺-Mnt25 and Li⁺-Mnt200: (a) ²⁹Si-MAS NMR spectra; (b) ²⁷Al-MAS NMR spectra, the reference mark (※) indicates spinning sidebands; (c) ⁷Li-MAS NMR spectra, the reference mark (※) signifies spinning sidebands; and (d) partial amplification from the ⁷Li-MAS NMR spectra.

upon heating to 200°C, Li⁺-Mnt25 and Li⁺-Mnt200 were selected for finer characterisation techniques (MAS NMR and XPS).

The ²⁹Si-MAS NMR patterns for Li⁺-Mnt25 and Li⁺-Mnt200 samples are illustrated in Fig. 6a. The ²⁹Si signal of Li⁺-Mnt25 displays a peak at approximately -92.7 ppm, indicative of tetrahedral silicon atoms connected to three other silicon atoms via oxygen (Alba *et al.*, 1998; Pavón and Alba, 2021). Upon heating to 200°C, the ²⁹Si signal's peak of Li⁺-Mnt200 shifts to approximately -95.3 ppm due to interlayer cations neutralising negative charges within structural unit layers and integrating into the crystal structure (Stuedel *et al.*, 2015). Moreover, the ²⁹Si peak widens, reflecting interlayer cation migration into tetrahedral positions post-heat treatment, leading to Si-O-Si angle changes (Alba *et al.*, 1998). The ²⁷Al-MAS NMR spectra for Li⁺-Mnt25 and Li⁺-Mnt200 are shown in Fig. 6b. The ²⁷Al signal in Li⁺-Mnt25 appears at ~7.5 and ~67.9 ppm, corresponding to octahedral Al (Al^{VI}) and tetrahedral Al (Al^{IV}), respectively (Takahashi *et al.*, 2008; Stuedel *et al.*, 2015). Additionally, the Al^{IV} signal intensity is notably lower than Al^{VI} due to the higher abundance of Al^{VI} (Reinholdt *et al.*, 2005; Stuedel *et al.*, 2015). Post-heating at 200°C, the Al^{IV} signal disappears, attributed to tetrahedral structure distortion from interlayer Li⁺ migration into the lattice (Stuedel *et al.*, 2015). Conversely, this effect is less pronounced with Li⁺ occupying octahedral vacancies, as a result of minimal interference from a small amount of migrating Li⁺ (Stuedel

et al., 2015). The spectra from ⁷Li-MAS NMR for Li⁺-Mnt25 and Li⁺-Mnt200 are shown in Fig. 6c. Both samples exhibit symmetrical powder sideband patterns, demonstrating a first-order quadrupolar interaction effect (Bodart *et al.*, 2018). For finer crystal structure insight, Fig. 6d shows an enlarged view of the ⁷Li-MAS NMR spectra. The main resonance signal of Li⁺-Mnt25 appears at ~0.2 ppm, consistent with interlayer Li⁺ (Pistiner and Henderson, 2003). Post-heating to 200°C, the ⁷Li signal of Li⁺-Mnt200 shifts by approximately -0.6 ppm, indicating octahedral Li⁺ presence (Hindshaw *et al.*, 2019).

The spectra from XPS depicting Li⁺-Mnt25 and Li⁺-Mnt200 are presented in Fig. 7. Notably, alterations in the chemical state on the mineral surface significantly influence the positions of the photoelectron peaks. The full spectrum analysis reveals peaks corresponding to O 1s, Si 2p, and Al 2p before and after heating (Fig. 7a). In the case of Li⁺-Mnt25, the Si 2p peak appears at ~102.7 eV, whereas after heating to 200°C, it is shifted to ~103.3 eV (Li⁺-Mnt200, Fig. 7b). This shift is attributed to the presumed entry of Li⁺ into the ditrigonal cavities of the tetrahedral layers, leading to an upwards shift in the Si 2p peak. The binding energies of Al 2p for Li⁺-Mnt25 and Li⁺-Mnt200 are situated at ~74.5 and ~75.4 eV, respectively (Fig. 7c). Earlier investigations suggest that the incorporation of Li⁺ into the aluminium-oxygen octahedron results in the shift of the Al 2p peak towards higher values (Zhong *et al.*, 2021). The Li 1s peak in Li⁺-Mnt25, located at ~57.3 eV, is hypothesised to represent interlayer

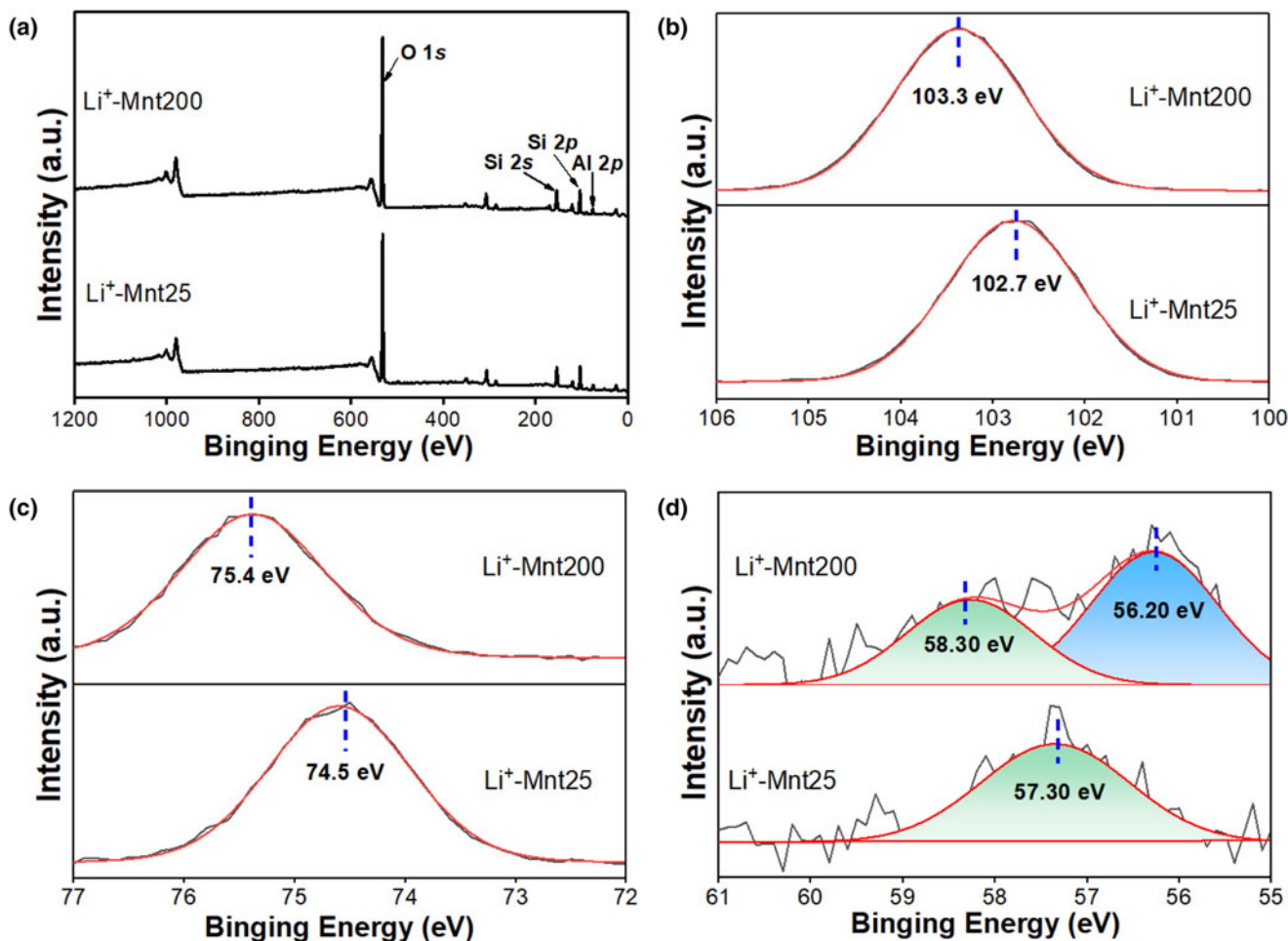


Figure 7. The XPS spectra of Li⁺-Mnt25 and Li⁺-Mnt200: (a) XPS survey; (b) Si 2p; (c) Al 2p; and (d) Li 1s.

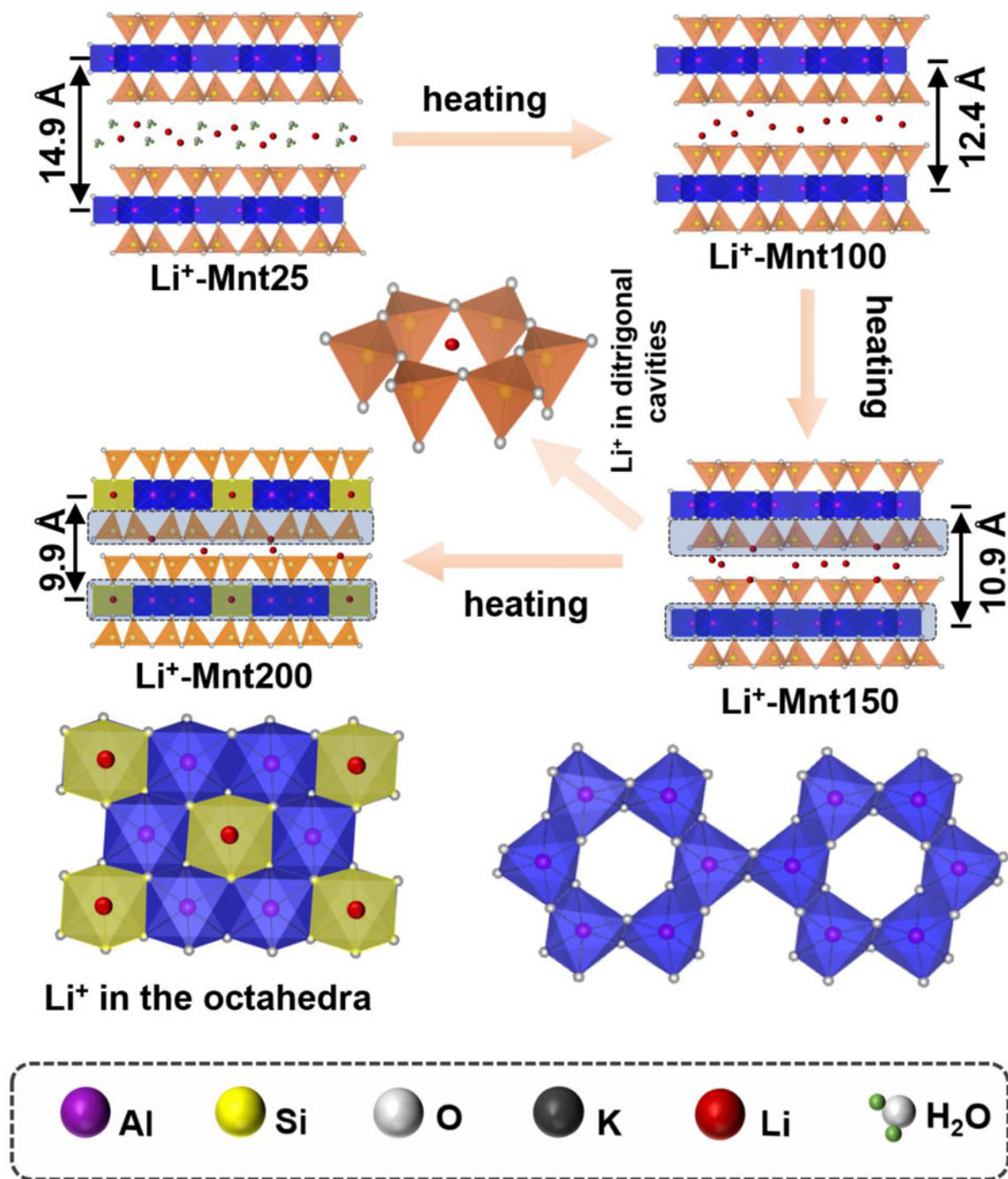


Figure 8. Diagram of Li^+ migration and occupation in montmorillonite during the heating process.

hydrated Li^+ (Fig. 7d). Upon heating to 200°C, the Li 1s peaks in Li^+ -Mnt200 appear at ~ 56.2 and ~ 58.3 eV, respectively (Fig. 7d). This discrepancy indicates that the former peak arises due to the dehydration of a portion of interlayer hydrated Li^+ into Li^+ at elevated temperatures. The latter phenomenon is attributed to the migration of Li^+ into the montmorillonite lattice, leading to an elevated binding energy of Li 1s (Shen *et al.*, 1990; Connell *et al.*, 2020).

Consequently, combined with the emerging OH stretching vibration (AlMgLi-OH) at ~ 3671 cm^{-1} upon heating montmorillonite at 200°C (Fig. 3d), the observed results of MAS NMR and

XPS confirm that interlayer Li^+ can migrate to the ditrigonal cavities and vacant octahedral sites of montmorillonite when heating at 200°C. In addition, it is explained that when the heating temperature reaches 200°C, Li^+ can migrate to vacant octahedral sites of montmorillonite through the ditrigonal cavities.

Migration and occupation of Li^+ in montmorillonite

The data from XRD, FTIR, MAS NMR and XPS concerning the migration and occupation of Li^+ in montmorillonite establishes

that Li^+ within the montmorillonite interlayer can infiltrate the montmorillonite lattice upon reaching a specific temperature (Fig. 8). This migration of Li^+ occurs through the three-step process. Initially, upon heating to 100°C , interlayer hydrated Li^+ undergoes dehydration; upon heating to 150°C , partial Li^+ can migrate into the ditrigonal cavities of the montmorillonite tetrahedral layers. With further temperature increase to 200°C , some Li^+ within the ditrigonal cavities proceeds to occupy previously vacant octahedrons in the montmorillonite, forming a local trioctahedral structure and leading to the complete collapse of the montmorillonite structural layer ($<10.0 \text{ \AA}$) (Fig. 8).

Conclusions

Under heating conditions, the mineral types and interlayer cations collectively influence the migration and occupation attributes of cations within minerals, thereby having an impact on mineral lattice structures. In the case of ilmenite, the 00l reflections exhibit little change after heating, whereas the $d_{(001)}$ values of montmorillonite display pronounced alterations. Specifically, the layer spacing of Li^+ -Mnt decreases to $<10.0 \text{ \AA}$, consistent with the complete collapse of montmorillonite, and the exchangeable Li^+ in Li^+ -Mnt gradually decreases with the increase of temperature, signifying Li^+ fixation by montmorillonite. Moreover, within the temperature range of $100\text{--}300^\circ\text{C}$, the OH vibrational bands and Si–O vibrational bands of Na^+ -Ilt, Li^+ -Ilt and Na^+ -Mnt remain relatively stable, whereas those of Li^+ -Mnt undergo modifications. Specifically, as the heating temperature reaches 150°C , the OH stretching and Si–O stretching vibrational bands of the Li^+ -Mnt series, shift towards higher values, accompanied by the intensity decrease of OH bending and Si–O bending vibrational bands. These changes are due to the entry of Li^+ into the ditrigonal cavities of montmorillonite. At 200°C , the emergence of a new OH stretching vibrational peak at $\sim 3671 \text{ cm}^{-1}$ is observed, possibly indicating the entry of Li^+ into montmorillonite vacant octahedrons and the formation of a local trioctahedral structure (AlMgLi–OH). MAS NMR analysis demonstrates that the chemical shifts of the ^{29}Si and ^7Li signals of Li^+ -Mnt200 are more negative in comparison to the Li^+ -Mnt25 sample. The ^{27}Al -MAS NMR spectrum reveals the disappearance of the Al^{IV} signal upon heating to 200°C . Furthermore, XPS spectra illustrate that, relative to the Li^+ -Mnt25 sample, Al 2p and Si 2p peaks in Li^+ -Mnt200 shift towards higher values, and the Li 1s peak emerges at $\sim 58.3 \text{ eV}$. These findings strongly support the migration of Li^+ into the crystal structure of montmorillonite under heating conditions.

Acknowledgements. The authors thank the financial support provided by the National Natural Science Foundation of China (42172043, 42202148) and the Fundamental Research Funds for the Central Universities, CHD (300102263301, 300102273203).

Competing interests. The authors declare none.

Supplementary material. The supplementary material for this article can be found at <https://doi.org/10.1180/mgm.2024.27>.

References

- Ai Q., Yang Z.J., Zeng X.Q., Zheng Y.L. and Hu P.Y. (2013) Study on the FTIR spectra of OH in olivines from Mengyin Kimberlite. *Spectroscopy and Spectral Analysis*, **33**, 2374–2378 [in Chinese with English abstract].
- Alba M.D., Alvero R., Becerro A.I., Castro M.A. and Trillo J.M. (1998) Chemical behavior of lithium ions in reexpanded Li-montmorillonites. *The Journal of Physical Chemistry B*, **102**, 2207–2213.
- Alvero R., Alba M.D., Castro M.A. and Trillo J.M. (1994) Reversible migration of lithium in montmorillonites. *Russian Journal of Physical Chemistry*, **98**, 7848–7853.
- Beaufort D., Berger G., Lachapagne J.C. and Meunier A. (2001) An experimental alteration of montmorillonite to a di-trioctahedral smectite assemblage at 100 and 200°C . *Clay Minerals*, **36**, 211–225.
- Bodart P.R., Delmotte L., Rigolet S., Brendlé J. and Gougeon R.D. (2018) $^7\text{Li}\{^{19}\text{F}\}$ TEDOR NMR to observe the lithium migration in heated montmorillonite. *Applied Clay Science*, **157**, 204–211.
- Cao Z., Wang Q. and Cheng H. (2021) Recent advances in kaolinite-based material for photocatalysts. *Chinese Chemical Letters*, **32**, 2617–2628.
- Chen T. and Wang H.J. (2007) Microstructure characteristics of illite from Chuanlinggou Formation of Changcheng System in Jixian County, Tianjin City. *Science in China (Series D: Earth Sciences)*, **50**, 1452–1458.
- Cheng H.F., Yang J., Liu Q.F., Zhang J.S. and Frost R.L. (2010) A spectroscopic comparison of selected Chinese kaolinite, coal bearing kaolinite and halloysite—A mid-infrared and near-infrared study. *Spectrochimica Acta*, **A77**, 856–861.
- Clementz D.M. and Mortland M.M. (1974) Properties of reduced charge montmorillonite: Tetra-alkylammonium ion exchange forms. *Clays and Clay Minerals*, **22**, 223–229.
- Connell J.G., Fuchs T., Hartmann H., Krauskopf T., Zhu Y.S., Sann J., Garcia-Mendez R., Sakamoto J., Tepavcic S. and Janek Jr. (2020) Kinetic versus thermodynamic stability of LLZO in contact with lithium metal. *Chemistry of Materials*, **32**, 10207–10215.
- Ebina T., Iwasaki T. and Jee A.C. (1999) XPS and DFT study on the migration of lithium in montmorillonite. *Clay science*, **10**, 569–581.
- Farmer V.C. and Russell J.D. (1967) Infrared absorption spectrometry in clay studies. *Clays and Clay Minerals*, **15**, 121–142.
- Gao X. (2017) *Clay Mineralogy*. Chemical Industry Press, China: Beijing, 230 pp. [in Chinese with English abstract].
- Gates W.P., Komadel P., Madejová J., Bujdák J., Stucki J.W. and Kirkpatrick R.J. (2000) Electronic and structural properties of reduced-charge montmorillonites. *Applied Clay Science*, **16**, 257–271.
- Gournis D., Lappas A., Karakassides M.A., Többsen D. and Moukarika A. (2008) A neutron diffraction study of alkali cation migration in montmorillonites. *Physics & Chemistry of Minerals*, **35**, 49–58.
- Greene-Kelly R. (1995) Dehydration of the montmorillonite minerals. *Mineralogical Magazine and Journal of the Mineralogical Society*, **30**, 604–615.
- Hindshaw R.S., Tosca R., Goût T.L., Farnan I., Tosca N.J. and Tipper E.T. (2019) Experimental constraints on Li isotope fractionation during clay formation. *Geochimica et Cosmochimica Acta*, **250**, 219–237.
- Jeldres R.I., Uribe L., Cisternas L.A., Gutierrez L., Leiva W.H. and Valenzuela J. (2019) The effect of clay minerals on the process of flotation of copper ores: A critical review. *Applied Clay Science*, **170**, 57–69.
- Karakassides M.A., Madejová J., Arvaiová B., Bourlinos A., Petridis D. and Komadel P. (1999) Location of Li(I), Cu(II) and Cd(II) in heated montmorillonite: evidence from specular reflectance infrared and electron spin resonance spectroscopies. *Journal of Materials Chemistry*, **9**, 1553–1558.
- Komadel P., Madejova J. and Bujdák J. (2005) Preparation and properties of reduced-charge smectites—A review. *Clays and Clay Minerals*, **53**, 313–334.
- Li R.H., Li X.Y., Li H.R., Zhao K.P. and Peng K. (2022) Structural characteristics of clay minerals and their progress in CO_2 adsorption. *Bulletin of the Chinese Ceramic Society*, **41**, 141–152 [in Chinese with English abstract].
- Liu Q.F., Yao X., Cheng H.F. and Frost R.L. (2012) An infrared spectroscopic comparison of four Chinese palygorskites. *Spectrochimica Acta*, **A96**, 784–789.
- Luca V. and Cardile C.M. (1988) Thermally induced cation migration in Na and Li montmorillonite. *Physics and Chemistry of Minerals*, **16**, 98–103.
- Madejová J., Arvaiová B. and Komadel P. (1999a) FTIR spectroscopic characterization of thermally treated Cu^{2+} , Cd^{2+} , and Li^+ montmorillonites. *Spectrochimica Acta*, **A55**, 2467–2476.
- Madejová J., Arvaiová B. and Komadel P. (1999b) FTIR spectroscopic characterization of thermally treated Cu^{2+} , Cd^{2+} , and Li^+ montmorillonites. *Spectrochimica Acta Part A: Molecular and Biomolecular Spectroscopy*, **55**, 2467–2476.
- Madejová J., Bujdák J., Petit S. and Komadel P. (2000) Effects of chemical composition and temperature of heating on the infrared spectra of Li-saturated dioctahedral smectites. (I) Mid-infrared region. *Clay Minerals*, **35**, 739–751.

- Madejová J., Pálková H. and Komadel P. (2006) Behaviour of Li^+ and Cu^{2+} in heated montmorillonite: Evidence from far-, mid-, and near-IR regions. *Vibrational Spectroscopy*, **40**, 80–88.
- Pavón E. and Alba M.D. (2021) Swelling layered minerals applications: A solid state NMR overview. *Progress in Nuclear Magnetic Resonance Spectroscopy*, **124–125**, 99–128.
- Pistiner J.S. and Henderson G.M. (2003) Lithium-isotope fractionation during continental weathering processes. *Earth and Planetary Science Letters*, **214**, 327–339.
- Qi C.W., Yin Y.S., Wu Z.H., Tao J.H., Wang T., Cheng S., Liu L. and Chen D.L. (2022) Study on mineral transformation during the combustion of Xiangxi Coal by FTIR, XRD and XPS. *Coal Conversion*, **45**, 18–25 [in Chinese with English abstract].
- Reinholdt M., Mieke-Brendle J., Delmotte L., Le Dred R. and Tuilier M.H. (2005) Synthesis and characterization of montmorillonite-type phyllosilicates in a fluoride medium. *Clay Minerals*, **40**, 177–190.
- Russell J.D. and Farmer V.C. (1964) Infrared spectroscopic study of the dehydration of montmorillonite and saponite. *Clay Minerals Bulletin*, **5**, 443–464.
- Schultz L.G. (1969) Lithium and potassium absorption, dehydroxylation temperature, and structural water content of aluminous smectites. *Clays and Clay Minerals*, **17**, 115–149.
- Shen M.L., Hrbek J., Sham T.K. and Xu G.Q. (1990) A soft X-ray study of the interaction of oxygen with Li. *Surface Science*, **234**, 324–334.
- Skoubris E.N., Chryssikos G.D., Christidis G.E. and Gionis V. (2013) Structural characterization of reduced-charge montmorillonites. Evidence based on FTIR spectroscopy, thermal behavior, and layer-charge systematics. *Clays and Clay Minerals*, **61**, 83–97.
- Stackhouse S. and Coveney P. (2002) Study of thermally treated lithium montmorillonite by Ab Initio methods. *Journal of Physical Chemistry B*, **106**, 12470–12477.
- Steudel A., Heinzmann R., Indris S. and Emmerich K. (2015) CEC and ^7Li MAS NMR study of interlayer Li^+ in the montmorillonite-beidellite series at room temperature and after heating. *Clays and Clay Minerals*, **63**, 337–350.
- Takahashi T., Kanhashi K. and Saito K. (2008) First evidence of multiple octahedral Al sites in Na-montmorillonite by ^{27}Al multiple quantum MAS NMR. *Clays and Clay Minerals*, **56**, 520–525.
- Tettenhorst R. (1962) Cation migration in montmorillonites. *American Mineralogist*, **47**, 769–773.
- Theng B.K.G., Hayashi S., Soma M. and Seyama H. (1997) Nuclear magnetic resonance and X-ray photoelectron spectroscopic investigation of lithium migration in montmorillonite. *Clays and Clay Minerals*, **45**, 718–723.
- Wang J., Wang J.X., Zeng F.G. and Wu X.L. (2011) Molecular simulations of crystal structure conformation, X-ray diffraction and infra-red spectrum in montmorillonites. *Acta Mineralogica Sinica*, **31**, 133–138 [in Chinese with English abstract].
- Warr L.N. (2020) Recommended abbreviations for the names of clay minerals and associated phases. *Clay Minerals*, **55**, 261–264. <https://doi.org/10.1180/clm.2020.30>.
- Wu Z., Zhao H., Zhou X., Wang Y., Zuo K. and Cheng H. (2022) Thermal Migration Behavior of Na^+ , Cu^{2+} and Li^+ in Montmorillonite. *Minerals*, **12**, 477.
- Xia L.Y., Zhong H., Liu G.Y., Huang Z.Q., Chang Q.W. and Li X.G. (2009) Comparative studies on flotation of illite, pyrophyllite and kaolinite with Gemini and conventional cationic surfactants. *Transactions of Nonferrous Metals Society of China*, **19**, 446–453.
- Zhao H., Wang Y. and Cheng H.F. (2023) Recent advances in lithium extraction from lithium-bearing clay minerals. *Hydrometallurgy*, **217**, 106025.
- Zhao X.Y. and Zhang Y.Y. (1990) *Clay Minerals and Analysis of Clay Minerals*. China Ocean Press, Beijing [in Chinese].
- Zhao K., Li G.R., Sun Z.X., Liu J.H., Zhou Y.P. and Xu L.L. (2022a) Role of clay minerals in uranium mining and metallurgy and uranium rich environment treatment. *Nonferrous Metals (Extractive Metallurgy)*, 111–120 [in Chinese with English abstract].
- Zhao Y., Ma W.P., Yang Y., Cui Y., Xu L., Luo C.G. and Wen H.J. (2022b) Experimental study on the sorption of Li^+ by clay minerals—implications for clay-type lithium deposit. *Acta Mineralogica Sinica*, **42**, 141–153 [in Chinese with English abstract].
- Zhong J., Lin S. and Yu J.G. (2021) Li^+ adsorption performance and mechanism using lithium/aluminum layered double hydroxides in low grade brines. *Desalination*, **505**, 114983.